Royer, C. (1985) Doctoral Thesis, University of Illinois at Urbana—Champaign, Urbana, IL.
Sardana, V., & Breslow, E. (1986) *Fed. Proc. 45*, 1538 (Abstr. 335).
Sardana, V., Carlson, J. D., Breslow, E., & Peyton, D. (1987) *Biochemistry 26*, 995–1003.
Scarlata, S., & Royer, C. A. (1986) *Biochemistry 25*, 4925–4929.
Sur, S. S., Rabbani, L. D., Libman, L., & Breslow, E. (1979) *Biochemistry 18*, 1026–1035.
Udgaonkar, J. B., & Baldwin, R. L. (1990) *Proc. Natl. Acad. Sci. U.S.A. 87*, 8197–8201.
Valdes, R., Jr., & Ackers, G. K. (1978) *Proc. Natl. Acad. Sci. U.S.A. 75*, 311–314.
Virmani-Sardana, V., & Breslow, E. (1983) *Int. J. Pept. Protein Res. 21*, 182–189.
Weber, G. (1951) *Biochem. J. 51*, 155–164.
Weber, G., & Drickamer, H. G. (1983) *Q. Rev. Biophys. 16*, 89–112.
Whittaker, B. A., & Allewell, N. M. (1984) *Arch. Biochem. Biophys. 234*, 585–590.
Whittaker, B. A., Allewell, N. M., Carlson, J., & Breslow, E. (1985) *Biochemistry 24*, 2782–2790.

Neutron and X-ray Scattering Studies on the Human Complement Protein Properdin Provide an Analysis of the Thrombospondin Repeat

Kathryn F. Smith,[‡] Kathleen F. Nolan,[§] Kenneth B. M. Reid,[§] and Stephen J. Perkins*[,‡]

Department of Biochemistry and Chemistry, Royal Free Hospital School of Medicine, Rowland Hill Street, London NW3 2PF, U.K., and MRC Immunochemistry Unit, Department of Biochemistry, University of Oxford, South Parks Road, Oxford OX1 3QU, U.K.

Received February 15, 1991; Revised Manuscript Received May 22, 1991

ABSTRACT: Properdin is a regulatory glycoprotein of the alternative pathway of the complement system of immune defense. It is responsible for the stabilization of the C3 convertase complex formed between C3b and the Bb fragment of factor B. Neutron and X-ray solution scattering experiments were performed on the dimeric and trimeric forms of properdin. These have R_G values of 9.1 and 10.7 nm, respectively. The scattering curves were compared with Debye sphere modeling simulations for properdin. Good agreements were obtained for models similar to published electron micrographs showing that the properdin trimer has a triangular structure with sides of 26 nm. Such a structure also accounted for sedimentation coefficient data on properdin. Primary structure analyses for mouse and human properdin have shown that this contains six homologous motifs known as the thrombospondin repeat (TSR), which is the second most abundant domain type found in the complement proteins. Sequences for these 12 TSRs were aligned with 19 others found in thrombospondin and the late complement components. Three distinct groups of TSRs were identified, namely, the TSRs found in thrombospondin and properdin, the TSRs mostly found at the N-terminus of the late complement components, and the TSRs found at the C-terminus of the late components. Averaged secondary structure predictions suggested that all three groups contain similar backbone structures with two amphipathic turn regions and one hydrophilic β-strand region. The mean dimensions of the TSRs of properdin in solution were determined to be approximately 4 nm × 1.7 nm × 1.7 nm, showing that these are elongated in structure.

The components of the complement system provide a major nonadaptive immune defense mechanism for its host (Reid, 1986; Law & Reid, 1988). These are activated in response to the challenge of foreign material in plasma. Complement activation proceeds through a series of limited proteolytic steps in one of two largely independent pathways, the classical and alternative pathways. The latter operates via a C3 "tick-over" mechanism, where the molecular structure of the target cell initiates an amplification loop (Lambris, 1990). Properdin is involved in the regulation of the alternative pathway by binding to and stabilizing the C3/C5 convertase complexes, C3b·Bb and $C3b_n$·Bb (Fearon & Austen, 1975; Medicus et al., 1976; Farries et al., 1987), and also by inhibiting the cleavage of C3b by factor I in the presence of factor H as a cofactor by interfering with the ability of factor I to bind C3b (Farries et al., 1988a). Properdin binds to the C-terminal region of the α-chain of C3 between residues 1402 and 1435 (Lambris et al., 1984; Daoudaki et al., 1988). There is also evidence that properdin binds to the Ba domain of factor B in order to facilitate the cleavage by factor D to form the C3 convertase complex, with the concomitent release of Ba (Farries et al., 1988b).

Mouse and human properdin each consist of a single polypeptide chain of 441–442 amino acids (Goundis & Reid, 1988; Nolan & Reid, 1990; Nolan et al., 1991a,b) with an apparent molecular weight of 55 000 when examined under dissociating conditions with or without reduction of disulfide bridges. Human properdin also contains up to 10% by weight of complex-type N-linked carbohydrate, corresponding to one or two oligosaccharides per monomer (Minta & Lepow, 1974; Farries

* To whom correspondence should be addressed.
‡ Royal Free Hospital School of Medicine.
§ University of Oxford.

0006-2960/91/0430-8000$02.50/0

& Atkinson, 1989). Six structural motifs homologous to a domain found in thrombospondin (the thrombospondin repeat; TSR)[1] have been identified in properdin, together with an N-terminal and C-terminal region (Goundis & Reid, 1988). In human properdin, each TSR is coded by a separate exon, except that the C-terminal segment also has half of the sixth TSR (Nolan et al., 1991b). Each TSR is about 58 residues in size. While circular dichroism experiments did not identify any α-helix or β-sheet structures (Smith et al., 1984), Fourier transform infrared spectroscopy indicated evidence for β-sheet and β-turn structures in the TSRs, and secondary structure predictions suggested that the β-turns could be correlated with the high proportions of Gly, Pro, Cys, and Ser residues in properdin (Perkins et al., 1989).

In plasma, human properdin exists as dimers (P_2; 26% of the total), trimers (P_3; 54%), and tetramers (P_4; 20%) at a total concentration of 5.7 ± 1.0 μg/mL, making it one of the least abundant complement components (Pangburn, 1989). Their specific activities decrease in the order $P_4 > P_3 > P_2$. A polymer of high molecular weight (P_n) had been identified as the "activated" form of properdin; however, this has now been shown to be an artifact of purification (Farries et al., 1987; Pangburn, 1989). Electron microscopy on properdin has shown that the monomer is a flexible rod-like structure of 26 nm in length and 2.5 nm in diameter (Smith et al., 1984). The quaternary structure of the P_2, P_3, and P_4 oligomers is formed by the association of these monomers into cyclic structures, probably by strong noncovalent interactions between the N-terminal and C-terminal regions of each monomer.

The TSR is the second most abundant domain found in the complement components. Since about 80% of properdin is constructed of TSRs, properdin is ideal for structural studies of the TSR. These data are required for structural studies of the late complement components, C6, C7, C8, and C9 (K. F. Smith, R. A. Harrison, and S. J. Perkins, unpublished data). The availability of the TSR sequences in these proteins now permits the computation of an optimal sequence alignment and the classifications of the TSRs and their physical properties. Small-angle scattering is a powerful technique for determining the arrangement of domains in multidomain proteins, especially if the analyses can be constrained by other sequence or structural information (Perkins, 1988a,b). For this, high-flux beam sources are required in view of the low solubility of properdin. Since the structure is studied under conditions close to physiological, this offers the important advantage that the dimensions of electron microscopy images of properdin (measured in vacuo) can be quantitatively tested. This analysis is independently verified by the use of hydrodynamic spheres to simulate experimental sedimentation coefficients. By these means, the arrangements of TSR domains in properdin P_2 and P_3 is determined, together with an assessment of its structure in the late complement components.

Materials and Methods

Solution Scattering Measurements on Properdin. Neutron-scattering data were obtained in four independent sessions on instruments D11 (Ibel, 1976) and D17 at the Institut Laue Langevin, Grenoble, France. Samples were measured at 20 °C in rectangular quartz Hellma cuvettes of 2-mm path length for samples in 80% and 100% ^2H_2O buffers and 1-mm path length for samples in H_2O buffers. These were also used for 280-nm absorbance measurements. Sample and buffer transmissions were measured in all cases for use in data reduction and analyses. In two sessions at instrument D11, the use of sample-to-detector distances of 2.00, 10.00, and 11.00 m with wavelengths λ of 1.001–1.002 nm resulted in a Q range of 0.05–1.1 nm^{-1} (where $Q = 4\pi \sin \theta/\lambda$; 2θ is the scattering angle; λ is the wavelength). Counting times ranged from between 2.5 and 4 h in 0% ^2H_2O buffers at 10 and 11 m for Guinier data (below) to between 5 and 8 min in 100% ^2H_2O buffers at 2 m for data at large Q (concentration = 0.43–1.16 mg/mL). In two sessions on instrument D17, the Q range used was 0.07–1.4 nm^{-1}, based on sample-to-detector distances of 1.40 and 3.46 m, with λ of 1.106 nm and a main beam-to-detector angle of 0°. Samples in 100% ^2H_2O buffers were counted for 1.6 h at 3.46 m and 0.8 h at 1.40 m (c = 0.34–0.42 mg/mL). Data reduction was performed by using standard Grenoble software (RNILS, SPOLLY, RGUIM, and RPLOT; Ghosh, 1989). A cadmium background is first subtracted from each scattering curve. The buffer background run was subtracted from that of the sample run, and the result was normalized for the detector response by using a water run from which an empty cell background had been subtracted.

X-ray scattering data were obtained with the low-angle solution scattering camera at station 8.2 (Towns-Andrews et al., 1989) at the SRS Daresbury, Warrington, U.K. Experiments were performed with beam currents of 118–133 mA and a ring energy of 2.00 GeV in one session. Samples were measured for 20 min at concentrations between 0.28 and 0.85 mg/mL. A 500-channel linear detector at a sample-to-detector distance of 3.83 m was used to give a Q range of 0.05–0.97 nm^{-1}. The Q range was calibrated using fresh, wet, slightly stretched rat tail collagen with a diffraction spacing of 67 nm. Samples were held in Perspex cells with a sample volume of 20 μL, contained within mica windows with a thickness of between 10 and 15 μm, in a temperature-controlled sample holder connected to a water bath at 20 °C. Buffers and samples were measured in alternation for equal times to minimize background subtraction errors. Since the data were prone to such errors, curves were only accepted for subsequent analyses if their Guinier plots were linear and led to reproducible data in repeated measurements. Curves were recorded in 10 time frames for subsequent checks for radiation damage, after which they were averaged. Data reduction was performed by using standard Daresbury software OTOKO (P. Bendall, J. Bordas, M. H. C. Koch, and G. R. Mant, EMBL Hamburg and SERC Daresbury Laboratory, unpublished software) to subtract the buffer runs from those of the samples. The scattering curves were normalized on the basis of an ion counter monitor positioned after the sample, and a detector response was measured for 6 h by using a uniform ^{55}Fe radioactive source.

The dimeric P_2, trimeric P_3, and tetrameric P_4 forms of properdin were prepared as described in Perkins et al. (1989). Neutron data were collected with either a buffer containing 0.15 M NaCl, 0.2 mM EDTA, and 12 mM phosphate, pH 7.4, or 0.5 M NaCl, 0.2 M glycine, and 12 mM phosphate, pH 7.4, on instrument D11, or a buffer containing 0.2 M NaCl and 12 mM phosphate at pH 7.0 on instrument D17. X-ray data were collected with a buffer containing 0.5 M NaCl, 0.2 M glycine, and 12 mM phosphate, pH 7.4. For the neutron experiments, samples were dialyzed at 6 °C into their buffers containing 0%, 80%, or 100% ^2H_2O for at least 36 h with four buffer changes. Sample concentrations c were determined by using an A_{280} coefficient (1%, 1 cm) of 23.9 calculated (Perkins, 1986) from the human sequence. This A_{280} assumed that there were two triantennary complex-type carbohydrate chains (28 residues) per properdin monomer, giving a total

[1] Abbreviations: TSR, thrombospondin repeat.

molecular weight M_r of 54 100 and a 10.6% carbohydrate content by weight. The latter is compatible with a biochemical determination of 9.8% carbohydrate (Minta & Lepow, 1974). By comparison, if the carbohydrates were biantennary, the M_r is 52 800 (8.3% carbohydrate by weight) and the A_{280} coefficient is 24.5. This A_{280} is higher than other estimates of 18 (Reid, 1981) and 17.1 (DiScipio, 1982) and is similar to a value of 23.4 calculated by Nolan and Reid (1990). The properdin samples showed a single band of approximately 55 000 in molecular weight on SDS-PAGE, in reducing conditions both before and after the solution scattering experiments. After solution scattering, the properdin samples did not exhibit significant changes in their original functional activity in an assay involving the lysis of rabbit red blood cells by a reagent dependent upon the addition of purified properdin (Reid, 1981).

Scattering Data Analyses. At small Q values, analyses of the scattering curves by the Guinier equation give R_G, the radius of gyration (which is a measure of macromolecular elongation), and $I(0)$, the forward-scattered intensity at zero Q (Glatter & Kratky, 1982):

$$\ln I(Q) = \ln I(0) - R_G^2Q^2/3$$

Absolute M_r values are obtained from the neutron $I(0)/c$ values measured in H_2O buffers, in which systematic errors of measurements are minimized (Jacrot & Zaccai, 1981). Relative M_r values are obtained from the X-ray $I(0)/c$ data provided that the buffer has the same electron density (Kratky, 1963). If one of the molecular dimensions is much larger than the other two, the radius of gyration of the cross section R_{XS} and the cross-sectional intensity at zero angle $[I(Q)Q]_{Q\to 0}$ are obtained in a larger Q range than that used in the R_G analyses:

$$\ln [I(Q)Q] = \ln [I(Q)Q]_{Q\to 0} - R_{XS}^2Q^2/2$$

In contrast variation studies, the neutron scattering match point of the protein [at which it is invisible: $I(0)$ is zero] is obtained experimentally from a plot of $\sqrt{I(0)}/cT_st$ against percent ^2H_2O (where T_s is the sample transmission and t is the path length). This can also be calculated from amino acid and carbohydrate compositions from sequence data, assuming that the protein volume is unhydrated with 10% of nonexchange of main-chain NH protons (Perkins, 1986). Generally, R_G values depend on the scattering density of the solvent, since different constituents within the protein have different scattering densities. This is described by a simplified form of the Stuhrmann equation (Ibel & Stuhrmann, 1976; Perkins, 1988a,b):

$$R_G^2 = R_C^2 + \alpha/\Delta\rho$$

where R_C is the R_G at infinite contrast, $\Delta\rho$ is the difference in scattering density ρ between the solute and solvent, and α is the radial inhomogeneity of scattering density fluctuations within the protein. α is positive if the outermost scattering densities are higher than those nearer the center.

In London, the neutron and X-ray scattering analyses were performed jointly by using a common interactive analysis and plotting program SCTPL3 (Perkins & Sim, 1986; A. S. Nealis and S. J. Perkins, unpublished software). Results were processed as a spreadsheet with Lotus 1-2-3 version 2.01 (Lotus Development, U.K.). Statistical analyses were performed with MINITAB version 6.1 (Ryan et al., 1985). Graphs were created with SIGMAPLOT version 3.1 (Jandel Scientific).

Modeling of Scattering and Hydrodynamic Data for Properdin. Calculations of scattering curves employed small overlapping Debye spheres to follow standard procedures (Glatter & Kratky, 1982) in application to neutron and synchrotron X-ray scattering data (Perkins & Weiss, 1983; Perkins, 1985; Perkins & Sim, 1986). To constrain the simulations, the unhydrated volume (66.8 nm^3) of properdin was calculated by using standard crystallographic volumes for amino acids and carbohydrates (Chothia, 1975; Perkins, 1986) for the 442 amino acid residues (Nolan et al., 1991a) and 28 presumed carbohydrate residues per monomer. This volume was subdivided into 128 cubes with sides of 0.8 nm per monomer in an array of 32 × 2 × 2 cubes for the simulations, and the total length of the monomer was 25.6 nm, in agreement with electron microscopy. The overlapping spheres of the same volume as the cubes were positioned at the centers of the 128 cubes. Neutron data corresponded largely to this unhydrated volume, since the hydration shell that surrounds the macromolecule is invisible by neutron contrast variation (Perkins, 1986). This means that partial specific volumes $\bar{v}$ are larger if calculated from neutron match points instead of by densitometric means. Neutron curve fitting was based on data in 0% ^2H_2O and in 80% and 100% ^2H_2O to correspond to high positive and high negative solute–solvent contrasts, respectively. A trial-and-error procedure was employed to test a wide range of different sphere models in order to determine which ones could be ruled out by the scattering data. Note that this method does not lead to the determination of a unique structure, although all the possible models are constrained by the total volume. The simulated neutron curves were corrected for wavelength spread and beam divergence (Cusack, 1981; Perkins & Weiss, 1983).

X-ray curve fitting (in a high positive solute–solvent contrast) is based on the hydrated volume. The total volume of 88.8 nm^3 per monomer was calculated as the sum of the dry volume and a hydration volume based on a standard hydration of 0.3 g of H_2O/gram of glycoprotein and an electrostricted water molecule volume of 0.0245 nm^3 in place of the free water volume of 0.0299 nm^3 (Perkins, 1986). This model was subdivided into 128 spheres as above, and the final Debye models were generated on the basis of cubes of side 0.885 nm.

Modeling of the sedimentation coefficient $s^\circ_{20,w}$ was based on the hydrated volume of 88.8 nm^3 as in the X-ray curve fitting. The frictional coefficient f was calculated from

$$f = M_r(1 - \bar{v}\rho_{20,w})/(N_a s^\circ_{20,w})$$

where $\rho_{20,w}$ is the density of water at 20 °C and N_a is Avogadro's constant. The $\bar{v}$ of properdin is calculated as 0.710 mL/g from its composition, with the consensus volumes in Perkins (1986) that allow for glycoprotein hydration. Calculations of f were performed by the modified Oseen tensor procedure using the program GENDIA (Garcia de la Torre & Bloomfield, 1977a, 1977b) and a low number of spheres. Hydrodynamic spheres required for the simulations of f do not overlap. In order to compensate for the volume of the void spaces between these nonoverlapping spheres, it was necessary to increase the total volume by resetting the hydration of 0.3 g of H_2O/gram of glycoprotein to 0.39 g (Perkins, 1989). The properdin monomer was formed from a line of 10 spheres with a sphere diameter of 2.644 nm, giving a total length of 26.44 nm, in accord with the length from electron microscopy.

Sequence Alignments and Secondary Structure Predictions. A total of 31 TSR sequences from 11 proteins were aligned manually and also with guidelines provided by the automatic multiple sequence alignment program MULTAL (Taylor, 1990). In the order shown in Figure 5, these were human thrombospondin (3 TSRs) (Lawler & Hynes, 1986; Wolf et al., 1990), mouse thrombospondin (2 of 3 TSRs) (Bornstein et al., 1990), mouse properdin (6 TSRs) (Goundis & Reid, 1988),

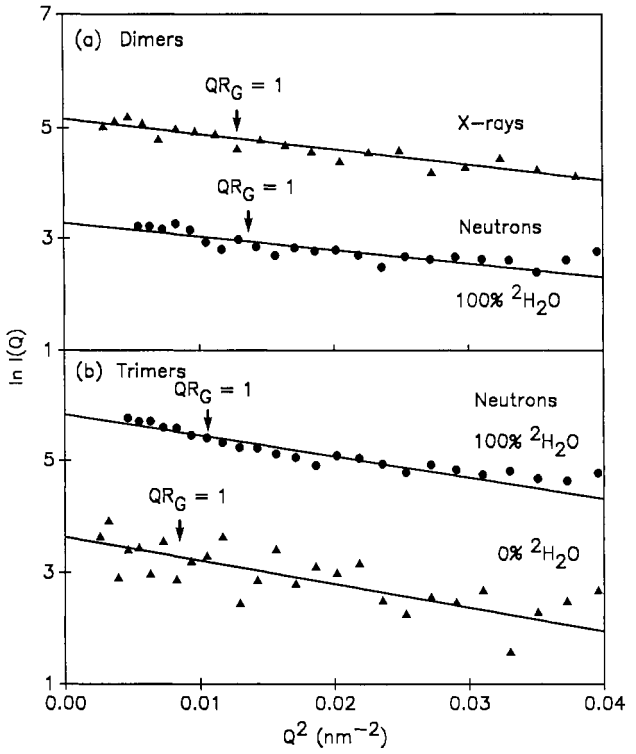

FIGURE 1: Guinier plots of properdin P_2 and P_3. In all cases, the condition $QR_G = 1$ is indicated by an arrow. (a) Data for P_2 in H_2O buffers by X-ray scattering and in ^2H_2O buffers by neutron scattering, at concentrations of 0.95 and 0.51 mg/mL, respectively. (b) Neutron data for P_3 in 100% and 0% ^2H_2O at concentrations of 1.21 and 1.14 mg/mL, respectively.

human properdin (6 TSRs) (Nolan et al., 1991a), thrombospondin-related anonymous protein (TRAP) from *Plasmodium falciparum* (1 TSR) (Robson et al., 1988), the late complement components human C6 (3 TSRs) (DiScipio & Hugli, 1989; Chakravarti et al., 1989; Haefliger et al., 1989), human C7 (2 TSRs) (DiScipio et al., 1988), human C8α (2 TSRs) (Rao et al., 1987), human C8β (2 TSRs) (Haefliger et al., 1987; Howard et al., 1987), human C9 (1 TSR) (DiScipio et al., 1984; Stanley et al., 1985), mouse C9 (1 TSR), and trout C9 (2 TSRs) (Stanley & Herz, 1987).

Secondary structure predictions based on the alignment of Figure 5 utilized the Robson and Chou–Fasman methods (Garnier et al., 1978; Chou & Fasman, 1978). The 31 predictions were averaged with the FORTRAN programs PREDRB7 and PREDCF (Perkins et al., 1988). Both programs produced the percentage frequency at which each residue was found in the helix, extended, turn, or coil conformation and the corresponding graphical output, while PREDRB7 also gave the averaged total score in centinats.

Results

Small-Angle Solution Scattering of P_2 and P_3. In order to obtain solution structure data on the arrangement of the six TSRs in properdin, P_2, P_3, and P_4 were studied by neutron scattering in three contrasts at concentrations between 0.3 and 1.2 mg/mL. Scattering data were, however, only accessible for P_2 and P_3 on instruments D11 and D17, since P_4 was found to possess too elongated a structure. In addition, P_3 could only be studied in 100% ^2H_2O buffers on D17 for reason of the lower neutron flux on D17, since only this buffer has a sufficiently low background. Guinier plots for P_2 and P_3 were linear over a Q range of 0.07–0.19 nm^{-1} (Figure 1). This Q range was thus employed for Guinier fits in acceptable QR_G ranges of 0.5–1.4 (P_2) and 0.7–2.0 (P_3).

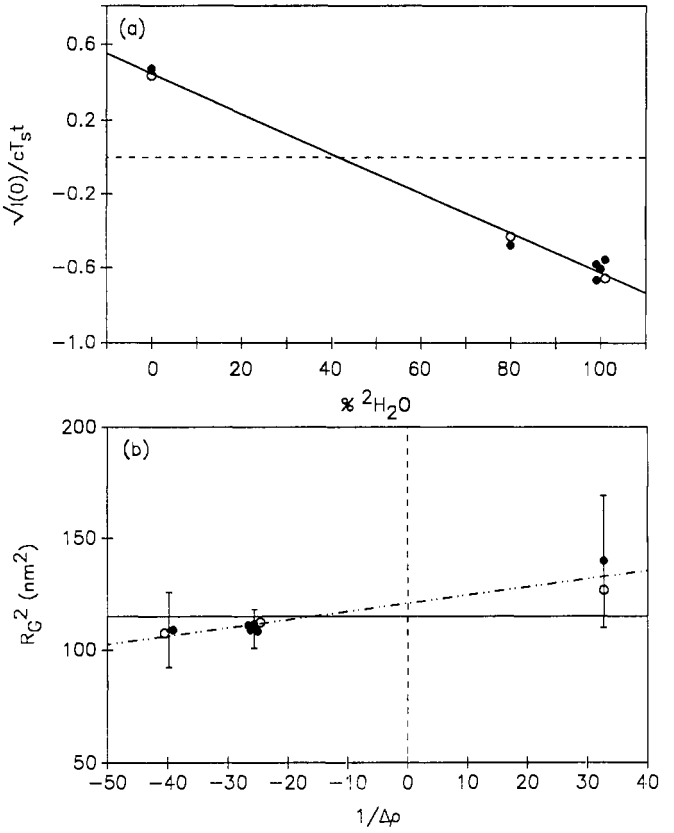

FIGURE 2: Neutron contrast variation analysis of P_3. A concentration range of 0.5–1.2 mg/mL was used. Buffers were either 0.15 M NaCl or 0.2 M NaCl in phosphate (●) (see Materials and Methods) or 0.5 M NaCl, 0.2 M glycine and 12 mM phosphate, pH 7.4 (○). (a) Match point determination of P_3 from a graph of $\sqrt{I(0)/cT_s}$ against the volume percentage of ^2H_2O. Regression gave a match point of 41.8 ± 1.9% ^2H_2O, corresponding to the intersection with the dashed line. (b) Stuhrmann plot of R_G^2 against the reciprocal solute–solvent contrast difference $\Delta\rho^{-1}$. The solid line corresponds to the mean R_G of 10.7 ± 0.5 nm. The dashed–dotted line corresponds to the regressed line and gives an R_C of 11.0 nm at zero $\Delta\rho^{-1}$ (dashed line) and a slope α of 4×10^{-3}. Statistical error bars from the Guinier analyses are shown.

Analyses of the Guinier neutron intensity $I(0)/c$ or radius of gyration R_G parameters showed that no dependences on protein concentrations or buffer compositions were observed (Figure 2). As a further check of the Guinier data, the molecular weights M_r for P_2 and P_3 were calculated from the $I(0)/c$ values measured in H_2O buffers, on the basis of an A_{280} coefficient of 23.9 (see Materials and Methods). The M_r values of 80000 ± 20000 (P_2, one value) and 150000 ± 30000 (P_3, two values) were in satisfactory agreement with the expected values from the primary sequence of 108200 and 162300, respectively. This calculation required the total of scattering lengths $\sum b$ in properdin normalized by the M_r, and this gave a $\sum b/M_r$ of 0.2237 fm in H_2O solutions, which is a typical value for globular proteins. For P_3, contrast variation showed that its match point was 41.8 ± 1.9% ^2H_2O (nine data points; Figure 2a). This agreed well with the prediction of 43.9% ^2H_2O from the amino acid and carbohydrate composition. For P_2, the limited availability of three data points in 0% and 100% buffers gave a comparable match point of 39.3 ± 1.2% ^2H_2O. The linear Guinier plots and the above agreements with known compositions showed that the scattering curves corresponded to monodisperse preparations of P_2 and P_3, as required for structural analyses.

The overall structure of P_3 is analyzed in Figure 2b, which shows the dependence of the neutron R_G data on the contrast.

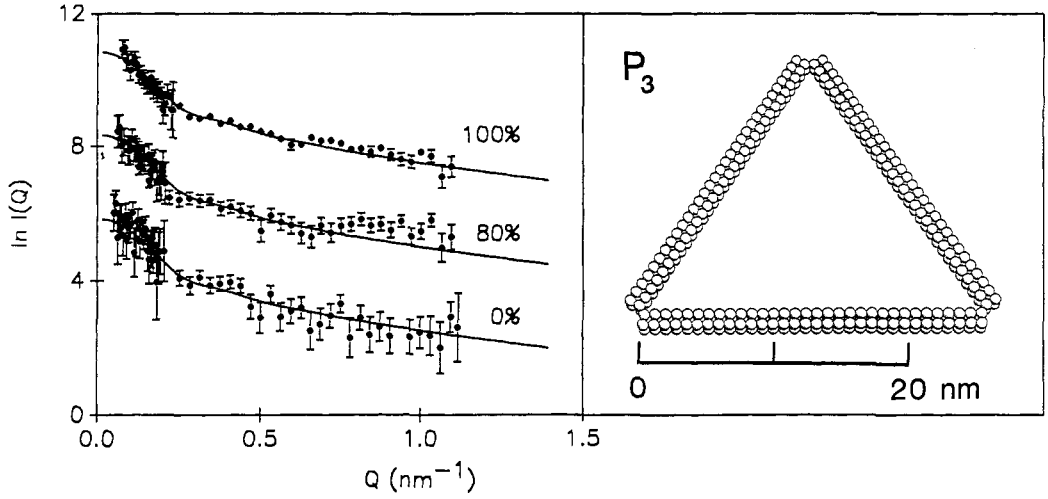

FIGURE 3: Neutron scattering curve simulations for P_3. The curve calculated from the model shown to the right (sphere diameter 0.8 nm; monomer of 32 × 2 × 2 spheres) is compared with the experimental curves measured in 100%, 80%, and 0% ^2H_2O buffers on instrument D11. The simulated curves were corrected for beam divergence and wavelength spread. The samples were at concentrations of 0.43, 0.40, and 1.1 mg/mL, respectively. Guinier R_G analyses were carried out in the Q range of 0.05–0.19 nm^{-1}. Error bars due to data counting statistics are shown.

As a result of low concentrations, the statistical errors of the R_G data were high. Even though an R_C of 11.0 ± 0.1 nm and a positive slope α of (4 ± 1) × 10^{-3} for P_3 could be determined from the nine values in Figure 2b by MINITAB analyses, the final R_G analysis was based on the mean R_G of 10.7 ± 0.5 nm. For P_2, the mean R_G value was 7.3 ± 1.6 nm from three measurements. Calculation of the elongation ratio R_G/R_0 (where R_0 is the R_G of the sphere with the same dry volume as P_2 or P_3) gave values of 3.0 ± 0.7 and 3.8 ± 0.2 for P_2 and P_3, respectively. Since the R_G/R_0 values for typical globular proteins are close to 1.28 (Perkins, 1988b), both P_2 and P_3 possess highly extended structures in solution, in common with many other complement components (Perkins et al., 1990a). In such cases, Guinier analyses of ln $I(Q)Q$ against Q^2 should provide the corresponding cross-sectional parameters $[I(Q)Q]_{Q\to 0}$ and R_{XS}. However, such plots were affected by poor signal–noise or buffer subtraction problems. The R_{XS} was estimated to be of the order of 0.6 ± 0.2 nm from data measured in 100% ^2H_2O buffers.

Synchrotron X-ray experiments were performed with P_2, P_3, and P_4 at concentrations of 0.29–0.89 mg/mL in order to extend the neutron analyses. Scattering curves were accepted for analyses if linear Guinier plots were obtained in Q ranges of 0.05–0.10 to 0.18–0.20 nm^{-1} (Figure 1a). As before, data for P_4 could not be analyzed. The mean R_G values were 9.1 ± 0.6 nm for P_2 (two values) and 11.6 ± 0.9 nm for P_3 (four values). The ratio of $I(0)/c$ values for P_2:P_3 was 1.00:1.49 (±17%), which is the value expected from their relative molecular weights. These data corresponded to measurements in high positive solute–solvent contrasts and as such could be compared with the neutron R_G values in 0% ^2H_2O buffers. Good agreements were found with the neutron R_G of 9 ± 2 nm for P_2 (one value) and 11.5 ± 0.4 nm for P_3 (two values) in H_2O, thus corroborating these analyses. However, there was evidence from time frame analyses of the P_3 data for on-going aggregation during beam exposure (to which the R_G data were insensitive), and these data were therefore not utilized in the curve-fitting analyses below.

Simulations of Scattering Curves for P_3. The use of small Debye spheres in molecular models permitted the interpretation of the scattering data for P_3 that were measured in the larger Q range between 0.2 and 1.1 nm^{-1}. From this, possible arrangements of the TSRs and the properdin monomers in P_3 could be deduced. Electron micrographs (Smith et al., 1984) had reported that properdin existed as cyclic structures, on the basis of a monomer that is 26 nm in length and 2.5–3 nm in width. These dimensions, however, led to a volume that is 2–3 times larger than that calculated from the composition. Here, a model for the monomer was taken to be 26 nm in length, with a width constrained by a dry volume close to 66.8 nm^3 (see Materials and Methods).

P_3 was most successfully modeled as three linear rods (32 spheres spaced 0.80 nm apart) with a circular cross section (2 × 2 spheres) that were arranged as the sides of an equilateral triangle. The dry volume of each rod was 65.5 nm^3. This dry model had an R_G of 10.9 nm, in very good agreement with the observed mean neutron R_G of 10.7 ± 0.5 nm. The simulated neutron curves agreed well with the neutron data in 100%, 80%, and 0% ^2H_2O (Figure 3), with satisfactory R values of 0.026, 0.047, and 0.059, respectively. R is a goodness-of-fit parameter that was defined in Smith et al. (1990). The view of this model is in good accord with observed electron micrographs of P_3.

Three other cyclic and extended models for P_3 were tested against the solution data. The use of an asymmetric cross section of 1 × 4 spheres in the triangular model led to worsened curve fits at large Q values (R of 0.036 in place of 0.026). The use of a circular ring of circumference 96 spheres and cross-section 2 × 2 spheres led to an R_G of 12.6 nm that was significantly larger than the experimental value and to worsened curve fits in the Q range between 0.2 and 0.4 nm^{-1}, although the curve fits at large Q were similar. Y-shaped models were tested in which the sides of the triangle were brought into contact with each other to result in a three-armed structure, such that the TSRs within each monomer were positioned in contact with TSRs in the neighbouring monomer. Here, however, the R_G value was much reduced to 8.1 nm, and the curve fits deteriorated (R of 0.032 in place of 0.026). These poorer curve fits with alternative arrangements of properdin monomers supported the proposal of a triangle model as the likely solution structure for P_3.

Simulations of Sedimentation Data for Properdin. For properdin, sedimentation coefficients $s^\circ_{20,w}$ of 5.0 S (DiScipio, 1982), 5.2 S (Minta & Kunar, 1976), and 5.1–5.3 S (Pensky et al., 1968) have been reported. These authors were not able to resolve P_2, P_3, and P_4 by ultracentrifugation. These $s^\circ_{20,w}$

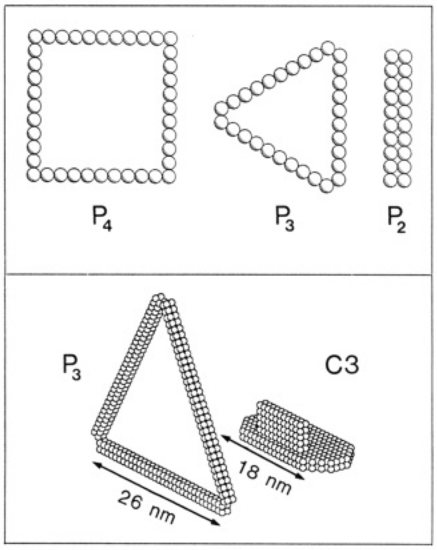

FIGURE 4: Low-resolution models of properdin. (Upper) Hydrodynamic models for tetrameric, trimeric, and dimeric properdin, based on spheres of diameter 2.664 nm. (Lower) The Debye model for trimeric properdin is shown in comparison with a simple two-domain model for complement component C3 from solution scattering analyses (Perkins et al., 1990b). It is stressed that such scattering curve models are only equivalent to the experimentally observed curves. While they do not correspond to a unique structure determination, the models will indicate the relative sizes of P_3 and C3.

data provide independent structural data of the degree of elongation of the P_2, P_3, and P_4 structures in solution. Simulations were performed with hydrodynamic sphere models to calculate the $s^{\circ}_{20,w}$ values of the models determined by solution scattering. The best agreements were based on a monomer length of 26 nm, constructed from a line of 10 spheres of diameter 2.644 nm. The P_2, P_3, and P_4 models were represented by two parallel lines, an equilateral triangle, and a square, respectively (Figure 4a). The predicted $s^{\circ}_{20,w}$ values were 5.08, 4.98, and 5.21 S in that order. The similarity of these values explained why the three forms cannot be distinguished by ultracentrifugation. These agreements are evidence that the length of the monomer was very close to that of 26 nm determined by solution scattering and electron microscopy. Calculations based on other lengths for the monomer showed that a typical error of ±0.2 S in the simulation (Perkins, 1989) corresponded to changes in the monomer length of ±2 nm.

Classification of TSR Sequences. In order to characterize the properties of a TSR within the properdin monomer, 31 full TSR sequences were aligned in Figure 5. This analysis was improved in comparison to that given in Perkins et al. (1989) because the intron/exon boundaries of the human and mouse thrombospondin genes (Wolf et al., 1990; Bornstein et al., 1990) and the human properdin gene (Nolan et al., 1991b) have been determined. These define the start and end of each TSR (Craik et al., 1982; Traut, 1988). The start of the TSR

```
                           1--------------17      18---24    25---------37  38---------50  51----58          Net
Group 1                                                                                                   charge
                                      ** *  *                 * *                  *            *
                             * **  ** *  **       ** *        * * *                * *          *     **
Thrombospondin (human)  SDSADDGWSPWSEWTSCSTS      CGNGIQQ    RGRSCDSLNNR       CEGSSVQTRT  CHIQE CDKRF  -2 (-1)
                          KQDGGWSHWSPWSSCSVT      CGDGVIT    RIRLCNSPSPQMN  GKPCEGEARETKA  CKKDA CPI    +2 (+3)
                            NGGWGPWSPWDICSVT      CGGGVQK    RSRLCNNPTPQFG  GKDCVGDVTENQI  CNKQD CPID   -1
Thrombospondin (mouse)  SDSADDGWSPWSEWTSCSAT      CGNGIQQ    RGRSCDSLNNR       CEGSSVQTRT  CHIQE CDKRF  -2 (-1)
                          KQDGGWSHWSPWSSCSVT      CGDGVIT    RIRLCNSPSPQMN  GKPCEGEARETKA  CKKDA CP     +2 (+3)
Properdin (mouse)           SPQWSAWSLWGPCSVT      CSEGSQL    RHRRCVGRGGQCS  ENVAPGTLEWQLQA CEDQPCCP     -1 ( 0)
                           EMGGWSEWGPWGPCSVT      CSKGTQI    RQRVCDNPAPKC   GGHCPGEAQQSQA  CDTQKTCP      0 (+1)
                           THGAWASWGPWSPRSGS      CLGGAQEPKETRSRSCSAPAPSHQPPGKPCSGPAYEHKA  CSGLPPCP     +3 (+6)
                           VAGGWGPWSPLSPCSVT      CGLGQTL    EQRTCDHPAPRHG  GPFCAGDATRNQM  CNKAVPCP     +1 (+3)
                           VNGEWEAWGKWSDCSRLRM SINCEGTPGQQS  RSRSCGDRKFN    GKPCAGKLQDIRH  CYNIHNCI     +4 (+6)
                           MKGSWSQWSTWSLCTPP      CSPNATRV   RQRLCTPLLPKYPPTVSMVEGQGEKNVTFWGTPRPLCE     +4
Properdin (human)           SPRWSLWSTWAPCSVT      CSEGSQL    RYRRCVGWNGQCS  GKVAPGTLEWQLQA CEDQQCCP     +1
                           EMGGWSGWGPWEPCSVT      CSKGTRT    RRRACNHPAPKC   GGHCPGQAQESEA  CDTQQVCP     +1 (+3)
                           THGAWATWGPWTPCSAS      CHGGPHEPKETRSRKCSAPEPSQKPPGKPCPGLAYEQRR  CTGLPPCP     +4 (+7)
                           VAGGWGPWGPVSPCPVT      CGLGQTM    EQRTCNHPVPQHG  GPFCAGDATRTHI  CNTAVPCP      0 (+3)
                           VDGEWDSWGEWSPCIRRNMKSISCQEIPGQQS  RGRTCRGRKFD    GHRCAGQQQDIRH  CYSIQHCP     +3 (+6)
                           LKGSWSEWSTWGLCMPP      CGPNPTRA   RQRLCTPLLPKYPPTVSMVEGQGEKNVTFWGRPLPRCE     +4
C6 N1 (human)              CFCDHYAWTQWTSCSKT      CNSGTQS    RHRQIVVDKYYQE   NFCEQICSKQETRECNWQR CP     +1 (+3)
TRAP (human)               KTASCGVWDEWSPCSVT      CGKGTRS    RKREIL         HEGCTSEIQEQ    CEEER CP     -2 (-1)

Group 2
                                   ** *  *                   * *                   *            *
                           * * **  ** *  * *      * *  *     * **    *** *         *            *     *
C6 N2 (human)              INCLLGDFGPWSDCDP       CIEKQS     KVRSVLRPSQFGG   QPCTEPLVAFQP  CIPSKLCK     +1
C7 N (human)               VNCQWDFYAPWSECNG       CTKTQT     RRRSVAVYGQYGG   QPCVGNAFETQS  CEPTRGCP     +1
C8α N (human)              VTCQLSNWSEWTDCFP       CQDKKY     RHRSLLQPNKFGG   TICSGDIWDQAS  CSSSTTCV      0 (+1)
C8b N (human)              IDCELSSWSSWTTCDP       CQKKRY     RYAYLLQPSQFHG   EPCNFSDKEVED  CVTNRPCR     -1 ( 0)
C9 N (human)               IDCRMSPWSEWSQCDP       CLRQMF     RSRSIEVFGQFNG   KRCTDAVGDRRQ  CVPTEPCE      0
C9 N (mouse)               IDCRMSPWSNWSECDP       CLKQRF     RSRSILAFGQFNG   KSCVDVLGDRQG  CETTQECE     -1
C9 N (trout)               VDCVWSRWSEWTPCNS       CTKIRH     RSRSVEVFGQFVG   KPCQGQPIGEQQA CTSDAVCE      0 (+1)

Group 3
                                  ** *  *                    * *                   *            *
                            ** ********** * *        *       * * **** *  *  *  *   * *          *
C6 C (human)               VDGQWGCWSSWSTCDA        TYKRS     RTRECNNPAPQRG  GKRCEGEKRQEED  CT           +1
C7 C (human)               VDGGWSCWSSWSPCVQ        GKKT      RSRECNNPPPSGG  GRSCVGETTESTQ  CE            0
C8α C (human)              ADGSWSCWSSWSVCRA        GIQE      RRRECDNPAPQNG  GASCPGRKVQTQA  C            +2
C8b C (human)              IDGKWNCWSNWSSCSG        RRKT      RQRQCNNPPPQNG  GSPCSGPASETLD  CS           +3
C9 C (trout)               EKGNWSCWAAWSGCSG        GKRI      RTRSCNT Q GLS  DATCRGDIVTEDY  C            +1

                              g  g  g                g             g             g      g

Robson                     bttttcttcttcttttt      ttttbbb    bbbbtbbtttttt  tbbbbttbbbbbt  tttttbbb
Chou-Fasman                ttttttbtttbtttttb      ttttbbb    atbbbbttttttt  ttttttaaaaaaa  battttt
                           <-----------t1--       --->‹--    -b1--->‹---t2  ---->
```

FIGURE 5: Alignment of 31 sequences for the thrombospondin repeat. A residue conservation greater than 70% within a group of sequences is denoted by ★ above the sequences, which are shaded if these are Cys residues. Residues conserved to better than 90% in all 31 sequences are indicated by two ★ above the sequences, and all are shaded. Putative glycosylation sites are underlined and indicated by g beneath the sequences. IQQ and RDG peptides are shown in the first and fourth sequences, and the last sequence, respectively. The averaged secondary structure prediction by the Robson and Chou–Fasman methods for the 31 sequences is shown beneath the sequences (b, β-sheet; a, α-helix; t, turn; c, coil). The letter is underlined if the prediction occurs in over 75% of the 31 sequences. To the right, the net charge found in each TSR is given assuming that the charged residues are D, E, R, and K; the bracketed figures correspond to the assumption that H is charged also, which, at a blood pH of 7.4, is not likely to be significant.

has now been displaced by 10 residues compared to that in Perkins et al. (1989). The alignment was also improved by the use of the automated multiple sequence alignment program MULTAL (Taylor, 1990). In order to facilitate the averaging of structural properties (Taylor, 1986; Perkins et al., 1988), gaps were minimized and homology was maximized between conserved or conservatively replaced residues. Figure 5 shows that eight residues were greater than 90% conserved in the 31 TSRs (Trp-8, Ser-9, Trp-11, Cys-14, Arg-25, Arg-27, Cys-41, and Cys-51).

The TSRs were readily subdivided into three groups on the basis of different Cys residue locations and different TSR lengths, in an extension of the initial survey of Patthy (1988). The closer similarities of the sequences within each group was confirmed by the MULTAL analyses using a range of sequence gap penalties. Groups 2 and 3 constituted the better defined families of sequences. Insertions or deletions in the group 1 sequences led to five contiguous peptide segments and four gap/insertion regions as indicated in Figure 5, of which the first segment (residues 1–17) exhibited the highest residue conservation in group 1.

A possible connectivity scheme for the three principal disulfide bridges in TSRs may be proposed from the alignment. It is likely that Cys-18 is linked to Cys-57 since both were missing in group 3 when compared to groups 1 and 2. Inspection of the four remaining Cys residues showed suggestively that Cys-41 and Cys-51 were both missing in the last TSR of human and mouse properdin, and therefore these appeared to be bridged in other sequences. Accordingly, Cys-14 may be linked either to Cys-29 (groups 1 and 3) or Cys-3 (group 2 and similar Cys residues in the C6 N1 and TRAP sequences of group 1). This scheme implied that Cys-7 in group 3 is unlinked within the TSR.

A total of nine putative NxT or NxS glycosylation sites were identified. An IQQ motif [factor $XIII_a$ binding; Bale et al. (1985)] was found in human and mouse thrombospondin. An RGD motif [cell surface receptor binding; Yamada (1989)] was found in trout C9 (Stanley & Herz, 1987). The structural motif WSxWS was found in 14 TSRs, occurring once or twice in all the protein sequences of groups 1, 2, and 3 except for those of TRAP and trout C9; this motif exists also in the cytokine hematopoietin receptor superfamily (Cosman et al., 1990). Within several TSRs in group 1 (but not in groups 2 or 3), a motif CSVTCGxGxxxRxR is found that is thought to function as a sulfated glycoconjugate-binding domain in properdin (Holt et al., 1990), although this motif is only conserved in full in the TRAP sequence and in three of the thrombospondin sequences.

The average of the 31 secondary structure predictions was computed, based on the Robson (β biased) and Chou–Fasman methods. Closely similar predictions to those reported previously (Perkins et al., 1989) were obtained. The total percentages of the four or three conformations present were identical. By the Robson method, these were α-helix, 0%; β-sheet, 38%; turn, 57%; and coil, 5%. The Chou–Fasman method gave α-helix, 16%; β-sheet, 18%; and turn, 66%. Again, two regions of high turn propensities could be identified (t_1 and t_2; residues 1–22 and 32–42) and one region of β-sheet (b_1; residues 23–31). While the two turn regions contained both hydrophilic and hydrophobic residues, nine out of the ten residues in the b_1 region were found to be hydrophilic. Further examination of the individual structure predictions supported the subdivision of TSRs into three groups. Unlike groups 1 and 3, residues 1–5 in group 2 were predicted as β-sheet. The predictions suggested that the b_1 region had different lengths, namely residues 23–28 in group 1, residues 19–33 in group 2, and residues 22–26 in group 3.

Discussion

Structure of Monomers in Properdin. Despite the low properdin concentrations, the use of high-flux beam sources (in particular at the Institut Laue Langevin) led to successful measurements of solution scattering curves. These were the most fruitful for the trimer P_3, which is the most abundant oligomer. Curve fitting was most successfully carried out in terms of open triangular structures in solution conditions close to physiological, with overall dimensions that were highly similar to the length of 26 nm reported on the basis of electron microscopy. Flexibility between the TSRs in each properdin monomer cannot, however, be ruled out by the scattering data.

One biochemical insight into the properties of properdin has been gained in this study. The calculated A_{280} coefficient of 23.9 from the primary structure is one-third higher than previously reported by biochemical determinations, as also reported in the calculation of Nolan and Reid (1990). Tests of this revised value led to satisfactory M_r values by solution scattering. This revision also implies that previous estimates of the concentration of properdin in plasma, initially 20–25 μg/mL (Minta et al., 1973) and then 5.7 μg/mL (Pangburn, 1989), should now be revised to 4.2 μg/mL.

Properdin has a high isoelectric point greater than 9.5. This is readily correlated with the excess of positive charges (R, K) over negative charges (D, E) in five of the six TSRs in the human sequence (Figure 5). It is possible that these charges may offer an explanation of these open cyclic structures, since the TSRs may repel each other. The three forms of properdin, P_2, P_3, and P_4, once isolated do not reequilibrate into a mixture. The structural studies suggest that the monomers associate between alternate N-terminal and C-terminal peptides at each end of each monomer. Inspection of their sequences suggest that the stability of these oligomers may be mediated by ionic interactions between up to 22 opposite charges in these regions.

The significance of the P_3 structure is shown by comparisons with the sizes of other proteins with which it interacts (Figure 4). The monomer length is 26 nm. This associates with C3b, which is of maximum length 18 nm (Perkins & Sim, 1986; Perkins et al., 1990b; Ikai et al., 1990). C3b interacts with properdin within a 34-residue segment of C3b (Daoudaki et al., 1988), which if in a maximally extended conformation would be of length 12 nm. These considerations show that it is reasonable to expect that for steric reasons more than one C3b molecule can interact with each of P_2, P_3, and P_4. In fact, Pangburn (1989) showed that the specific activity of properdin decreases in the order $P_4 > P_3 > P_2$.

Structure of TSRs in Properdin. Structural information on TSRs have been deduced from this study. Since TSRs exist in single copies in the late complement components, and since the multiple TSRs in thrombospondin and five out of the six TSRs in properdin are encoded by separate exons, it can be inferred that each TSR constitutes an independently folded protein structure. While TSRs are the second most abundant complement sequence motif, analysis shows that these may be subdivided into three groups. In contrast, the most abundant complement motif, the short complement (or consensus) repeat, is readily considered as a single group of sequences (Perkins et al., 1988).

The TSRs in these three groups exhibit distinct differences in Cys contents, lengths, and overall charges. Since similar locations for gaps and insertions could be proposed in the 31 TSR sequences (Figure 5), the protein backbone structure is expected to be similar in all three groups, even though the TSR

in the late complement components is smaller. In support of this premise, only minor differences were seen between the groups in the structure predictions. The principal characteristics of the three groups are summarized:

(i) Group 1, which included the thrombospondin and properdin sequences and interestingly the first N-terminal TSR of C6, contained complex arrangements of between four and seven Cys. These occurred most frequently at Cys-14, -18, -29, -41, -51, and -57. The TSR was 58 residues in length, 19 of which were conserved to better than 70%. The properdin TSRs generally displayed two to four positive charges on average, depending on the ionization state of about two His residues per TSR.

(ii) Group 2 corresponded to the N-terminal TSRs of the late complement components except for that above in C6. These contained six Cys as in group 1, except that Cys-29 is replaced by Cys-3. Most notably, the well-conserved Trp-5, Cys-29, and Gly-43 residues in group 1 were poorly conserved in group 2, while several well-conserved residues, 33–37, in group 2 do not have their counterpart in group 1. The average length of the group 2 TSR was 55 residues, 23 of which were conserved to better than 70%. These TSRs were generally uncharged.

(iii) Group 3 corresponded to the C-terminal TSRs in the late components. This group contained five Cys residues at Cys-7, -14, -29, -41, and -51. This group exhibited the highest residue conservation and the shortest sequences; the average length was 47 residues, 25 of which were conserved to better than 70%. While Trp-5, Cys-29, and Gly-43 are now well conserved as in group 1, many conserved residues in group 3 have no counterpart in group 1. These TSRs exhibited low positive charges.

To interpret the solution scattering analyses, the dry volume of each TSR can be calculated from amino acid compositions (Perkins, 1986). The average volume of the TSRs of group (excepting TRAP), group 2, and group 3 without carbohydrates were 8.2 ± 0.6, 7.6 ± 0.6, and 6.3 ± 0.3 nm^3, respectively. If the TSR were spherical, its diameter would be 2.5, 2.4, and 2.3 nm, respectively, in the three groups. The average volume for human and mouse properdin of the N- and C-terminal polypeptides was found to be 6.64 ± 0.18 and 4.16 ± 0.08 nm^3, respectively. If spherical, these would have diameters of 2.4 and 2.0 nm, respectively.

The length of a properdin monomer is 26 nm. If each of the six group 1 TSRs found in properdin are assumed to be spherical in shape, together with the N-terminal and C-terminal peptides, the sum of the eight diameters gives a total length of 19 nm if all eight structures were positioned in a linear arrangement. Since this length is notably shorter than the observed length, this shows that the TSR has an elongated structure. Its length can range between 3.25 and 4.3 nm, depending on the presumed structure of the N-terminal and C-terminal regions (Perkins et al., 1989). On the basis of the scattering curve fits at large Q for properdin, the cross-sectional dimensions of the TSR are compact at average values of 1.7 nm × 1.7 nm. On this scale, each TSR is equivalent to 16 spheres (Figure 3). Similar overall dimensions are expected for the TSRs found in the late complement components.

Acknowledgments

We thank the Wellcome Trust for support and the Science and Engineering Research Council for use of the Synchrotron Research Source (Daresbury) and the Institut Laue Langevin (Grenoble). Mr. A. S. Nealis, Ms. J. Parsons, and Drs. W. Bras, A. de Geyer, D. Goundis, and J. Torbet are gratefully thanked for support and assistance. A preliminary account of this work was given at the 635th Biochemical Society Meeting, July 17–19, 1990, Aberdeen, U.K.

Registry No. Properdin, 11016-39-0.

References

Bale, M. D., Westrick, L. G., & Mosher, D. F. (1985) *J. Biol. Chem. 260*, 7502–7508.

Bornstein, P., Alfi, D., Devarayalu, S., Framson, P., & Li, P. (1990) *J. Biol. Chem. 265*, 16691–16698.

Chakravarti, D. N., Chakravarti, B., Parra, C. A., & Müller-Eberhard, H. J. (1989) *Proc. Natl. Acad. Sci. U.S.A. 86*, 2799–2803.

Chothia, C. (1975) *Nature (London) 254*, 304–308.

Chou, P. Y., & Fasman, G. D. (1978) *Adv. Enzymol. Relat. Areas Mol. Biol. 47*, 45–148.

Cosman, D., Lyman, S. D., Idzerda, R. L., Beckmann, M. P., Park, L. S., Goodwin, R. G., & March, C. J. (1990) *Trends Biochem. Sci. 15*, 265–270.

Craik, C. S., Sprang, S., Fletterick, R., & Rutter, W. J. (1982) *Nature (London) 299*, 180–182.

Cusack, S. (1981) *J. Mol. Biol. 145*, 539–541.

Daoudaki, M. A., Becherer, J. D., & Lambris, J. D. (1988) *J. Immunol. 140*, 1577–1580.

DiScipio, R. G. (1982) *Mol. Immunol. 19*, 631–635.

DiScipio, R. G., & Hugli, T. E. (1989) *J. Biol. Chem. 264*, 16197–16206.

DiScipio, R. G., Gehring, M. R., Podack, E. R., Kan, C. C., Hugli, T. E., & Fey, G. H. (1984) *Proc. Natl. Acad. Sci. U.S.A. 81*, 7298–7302.

DiScipio, R. G., Chakravarti, D. N., Müller-Eberhard, H. J., & Fey, G. H. (1988) *J. Biol. Chem. 263*, 549–560.

Farries, T. C., & Atkinson, J. P. (1989) *J. Immunol. 142*, 842–847.

Farries, T. C., Finch, J. T., Lachmann, P. J., & Harrison, R. A. (1987) *Biochem. J. 243*, 507–517.

Farries, T. C., Lachmann, P. J., & Harrison, R. A. (1988a) *Biochem. J. 252*, 47–54.

Farries, T. C., Lachmann, P. J., & Harrison, R. A. (1988b) *Biochem. J. 253*, 667–675.

Fearon, D. T., & Austen, K. F. (1975) *J. Exp. Med. 142*, 856–863.

Garcia de la Torre, J., & Bloomfield, V. A. (1977a) *Biopolymers 16*, 1747–1761.

Garcia de la Torre, J., & Bloomfield, V. A. (1977b) *Biopolymers 16*, 1779–1793.

Garnier, J., Osguthorpe, D. J., & Robson, B. (1978) *J. Mol. Biol. 120*, 97–120.

Ghosh, R. E. (1989) *Internal Publication 89GH02T*, Institut Laue Langevin, Grenoble, France.

Glatter, O., & Kratky, O. (Eds.) (1982) *Small-Angle X-ray Scattering*, Academic Press, New York.

Goundis, D., & Reid, K. B. M. (1988) *Nature (London) 335*, 82–85.

Haefliger, J.-A., Tschopp, J., Nardelli, D., Wahli, W., Kocher, H. P., Tosi, M., & Stanley, K. K. (1987) *Biochemistry 26*, 3551–3556.

Haefliger, J.-A., Tschopp, J., Vial, N., & Jenne, D. E., (1989) *J. Biol. Chem. 264*, 18041–18051.

Holt, G. D., Pangburn, M. K., & Ginsburg, V. (1990) *J. Biol. Chem. 265*, 2852–2855.

Howard, O. M. Z., Rao, A. G., & Sodetz, J. M. (1987) *Biochemistry 26*, 3565–3570.

Ibel, K. (1976) *J. Appl. Crystallogr. 9*, 269–309.

Ibel, K., & Stuhrmann, H. B. (1975) *J. Mol. Biol. 93*, 225–266.

Ikai, A., Nishigai, M., Saito, A., Sinohara, H., Muto, Y., & Arata, Y. (1990) *FEBS Lett. 260*, 291–293.
Jacrot, B., & Zaccai, G. (1981) *Biopolymers 20*, 2413–2426.
Kratky, O. (1963) *Prog. Biophys. Chem. 13*, 105–173.
Lambris, J. D. (Ed.) (1990) *Curr. Top. Microbiol. Immunol. 153*, 1–251.
Lambris, J. D., Alsenz, J., Schulz, T. F., & Dierich, M. P. (1984) *Biochem. J. 217*, 323–326.
Law, S. K. A., & Reid, K. B. M. (1988) *Complement*, IRL Press, Oxford, U.K.
Lawler, J., & Hynes, R. O. (1986) *J. Cell Biol. 263*, 5495–5498.
Medicus, R. G., Götze, O., & Müller-Eberhard, H. J. (1976) *J. Exp. Med. 144*, 1076–1093.
Minta, J. O., & Lepow, I. H. (1974) *Immunochemistry 11*, 361–368.
Minta, J. O., & Kunar, E. S. (1976) *J. Immunol. 116*, 1099–1104.
Minta, J. O., Goodkofsky, I., & Lepow, I. H. (1973) *Immunochemistry 10*, 341–350.
Nolan, K. F., & Reid, K. B. M. (1990) *Biochem. Soc. Trans. 18*, 1161–1162.
Nolan, K. F., Schwaeble, W., Kaluz, S., Dierich, M. P., & Reid, K. B. M. (1991a) *Eur. J. Immunol. 21*, 771–776.
Nolan, K. F., Goundis, D., Kaluz, S., & Reid, K. B. M. (1991b) *Biochem. J.* (submitted).
Pangburn, M. K. (1989) *J. Immunol. 142*, 202–207.
Patthy, L. (1988) *J. Mol. Biol. 202*, 689–696.
Pensky, J., Hinz, C. F., Todd, E. W., Wedgwood, R. J., Boyer, J. T., & Lepow, I. H. (1968) *J. Immunol. 100*, 142–158.
Perkins, S. J. (1985) *Biochem. J. 228*, 13–26.
Perkins, S. J. (1986) *Eur. J. Biochem. 157*, 169–180.
Perkins, S. J. (1988a) *Biochem. J. 254*, 313–327.
Perkins, S. J. (1988b) *New Compr. Biochem. 18B*, 143–264.
Perkins, S. J. (1989) In *Dynamic Properties of Biomolecular Assemblies* (Harding, S. E. & Rowe, A. J., Eds.) Chapter 15, pp 226–245, Royal Society of Chemistry, London.
Perkins, S. J., & Weiss, H. (1983) *J. Mol. Biol. 168*, 847–866.
Perkins, S. J., & Sim, R. B. (1986) *Eur. J. Biochem. 157*, 155–168.
Perkins, S. J., Haris, P. I., Sim, R. B., & Chapman, D. (1988) *Biochemistry 27*, 4004–4012.
Perkins, S. J., Nealis, A. S., Haris, P. I., Chapman, D. Goundis, D., & Reid, K. B. M. (1989) *Biochemistry 28*, 7176–7182.
Perkins, S. J., Smith, K. F., & Nealis, A. S. (1990a) *Biochem. Soc. Trans. 18*, 1151–1154.
Perkins, S. J., Nealis, A. S., & Sim, R. B. (1990b) *Biochemistry 29*, 1167–1175.
Rao, A. G., Howard, O. M. Z., Ng, S. C., Whitehead, A. S., Colten, H. R., & Sodetz, J. M. (1987) *Biochemistry 26*, 3556–3564.
Reid, K. B. M. (1981) *Methods Enzymol. 80*, 143–150.
Reid, K. B. M. (1986) *Essays Biochem. 27*, 27–68.
Robson, K. B. H., Hall, J. R. S., Jennings, M. W., Harris, T. J. R., Marsh, K., Newbold, C. I., Tate, V. E., & Weatherall, D. J. (1988) *Nature (London) 335*, 79–82.
Ryan, B. F., Joiner, B. L., & Ryan, T. A. (1985) *Minitab Handbook*, 2nd ed., PWS-Kent Publishing Company, Boston.
Smith, C. A., Pangburn, M. K., Vogel, C.-W., & Müller-Eberhard, H. J. (1984) *J. Biol. Chem. 259*, 4582–4588.
Smith, K. F., Harrison, R. A., & Perkins, S. J. (1990) *Biochem. J. 267*, 203–212.
Stanley, K. K., & Herz, J. (1987) *EMBO J. 6*, 1951–1957.
Stanley, K. K., Kocher, H. P., Luzio, J. P., Jackson, P., & Tschopp, J. (1985) *EMBO J. 4*, 375–382.
Taylor, W. R. (1986) *J. Mol. Biol. 188*, 233–258.
Taylor, W. R. (1990) *Methods Enzymol. 183*, 456–474.
Towns-Andrews, E., Berry, A., Bordas, J., Mant, G. R., Murray, P. K., Roberts, K., Sumner, I., Worgan, J. S., Lewis, R., & Gabriel, A. (1989) *Rev. Sci. Instrum. 60*, 2346–2349.
Traut, T. W. (1988) *Proc. Natl. Acad. Sci. U.S.A. 85*, 2944–2948.
Wolf, F. W., Eddy, R. L., Shows, T. B., & Dixit, V. M. (1990) *Genomics 6*, 685–691.
Yamada, K. M. (1989) *Curr. Opin. Cell Biol. 1*, 956–963.